3-D linear inversion of gravity data: method and application to Basse-Terre volcanic island, Guadeloupe, Lesser Antilles

Anne Barnoud, Olivier Coutant, Claire Bouligand, Hendra Gunawan, Sébastien Deroussi

Geophysical Journal International

Geophys. J. Int. (2016) **205,** 562–574
GJI Gravity, geodesy and tides

doi: 10.1093/gji/ggw030

3-D linear inversion of gravity data: method and application to Basse-Terre volcanic island, Guadeloupe, Lesser Antilles

Anne Barnoud,[1,2] Olivier Coutant,[1,2] Claire Bouligand,[1,2] Hendra Gunawan[3] and Sébastien Deroussi[4]

[1] *Université Grenoble Alpes, ISTerre, F-*38041 *Grenoble, France. E-mail: anne.barnoud@gmail.com*
[2] *CNRS, ISTerre, F-*38041 *Grenoble, France*
[3] *Center for Volcanology and Geological Hazard Mitigation (PVMBG), JI Diponegoro No* 57, *Bandung, Indonesia*
[4] *Institut de Physique du Globe de Paris, Sorbonne Paris Cité, Univ. Paris Diderot, UMR* 7154 *CNRS, F-*75005 *Paris, France*

Accepted 2016 January 18. Received 2016 January 16; in original form 2015 September 3

SUMMARY

We use a Bayesian formalism combined with a grid node discretization for the linear inversion of gravimetric data in terms of 3-D density distribution. The forward modelling and the inversion method are derived from seismological inversion techniques in order to facilitate joint inversion or interpretation of density and seismic velocity models. The Bayesian formulation introduces covariance matrices on model parameters to regularize the ill-posed problem and reduce the non-uniqueness of the solution. This formalism favours smooth solutions and allows us to specify a spatial correlation length and to perform inversions at multiple scales. We also extract resolution parameters from the resolution matrix to discuss how well our density models are resolved. This method is applied to the inversion of data from the volcanic island of Basse-Terre in Guadeloupe, Lesser Antilles. A series of synthetic tests are performed to investigate advantages and limitations of the methodology in this context. This study results in the first 3-D density models of the island of Basse-Terre for which we identify: (i) a southward decrease of densities parallel to the migration of volcanic activity within the island, (ii) three dense anomalies beneath Petite Plaine Valley, Beaugendre Valley and the Grande-Découverte-Carmichaël-Soufrière Complex that may reflect the trace of former major volcanic feeding systems, (iii) shallow low-density anomalies in the southern part of Basse-Terre, especially around La Soufrière active volcano, Piton de Bouillante edifice and along the western coast, reflecting the presence of hydrothermal systems and fractured and altered rocks.

Key words: Inverse theory; Gravity anomalies and Earth structure; Volcanic hazards and risks.

1 INTRODUCTION

Geophysical imaging of volcanoes and volcanic islands is a particularly challenging exercise because of their structural complexities and potential difficult accesses. Distribution of geophysical data is usually uneven and often displays large gaps such as over the highest peaks. Geological constraints that would help the interpretation are often lacking. On the other hand, interpretation of geophysical data is complicated by the effect of the rugged topography, the 3-D geometry of structures, and the existence of strong heterogeneities in the subsurface. In addition, inversion of gravimetric data suffers from the intrinsic non uniqueness of the solution. Nevertheless, gravity inversions have been widely used in volcanic areas and gave convincing results about the structures of the edifices. To do so, authors used diverse approaches to regularize the inverse problem and achieve uniqueness.

A common strategy to invert gravity data is to produce smooth density models by including different types of *a priori* information in weighting matrices (e.g. Green 1975; Li & Oldenburg 1998; Boulanger & Chouteau 2001). Looking for compact solutions can also be used as a constraint with criteria of minimum volume (Last & Kubik 1983) or minimum moment of inertia (Guillen & Menichetti 1984). Another method is to fix the density contrasts and seek for geometrical features such as interfaces or extent and shape of causative bodies (e.g. Pedersen 1979; Barbosa & Silva 1994; Camacho *et al.* 2000). These different regularization methods have been applied to many volcanic areas. Camacho *et al.* (1997) used probability density functions as in Tarantola & Valette (1982) to obtain a smooth model of São Miguel island (Azores). Cella *et al.* (2007) followed the method proposed by Li & Oldenburg (1998) adapted for their data sets from the Somma-Vesuvius volcano (Italy). Linde *et al.* (2014) successively minimized L2 and L1 norms to recover sharp transitions within the Stromboli volcano (Italy) in addition to a first smooth model. In other studies, authors predefined density contrasts and sought for interfaces (Camacho *et al.* 2011) or shapes (Montesinos *et al.* 2006; Camacho *et al.* 2007, 2009; Represas *et al.* 2012).

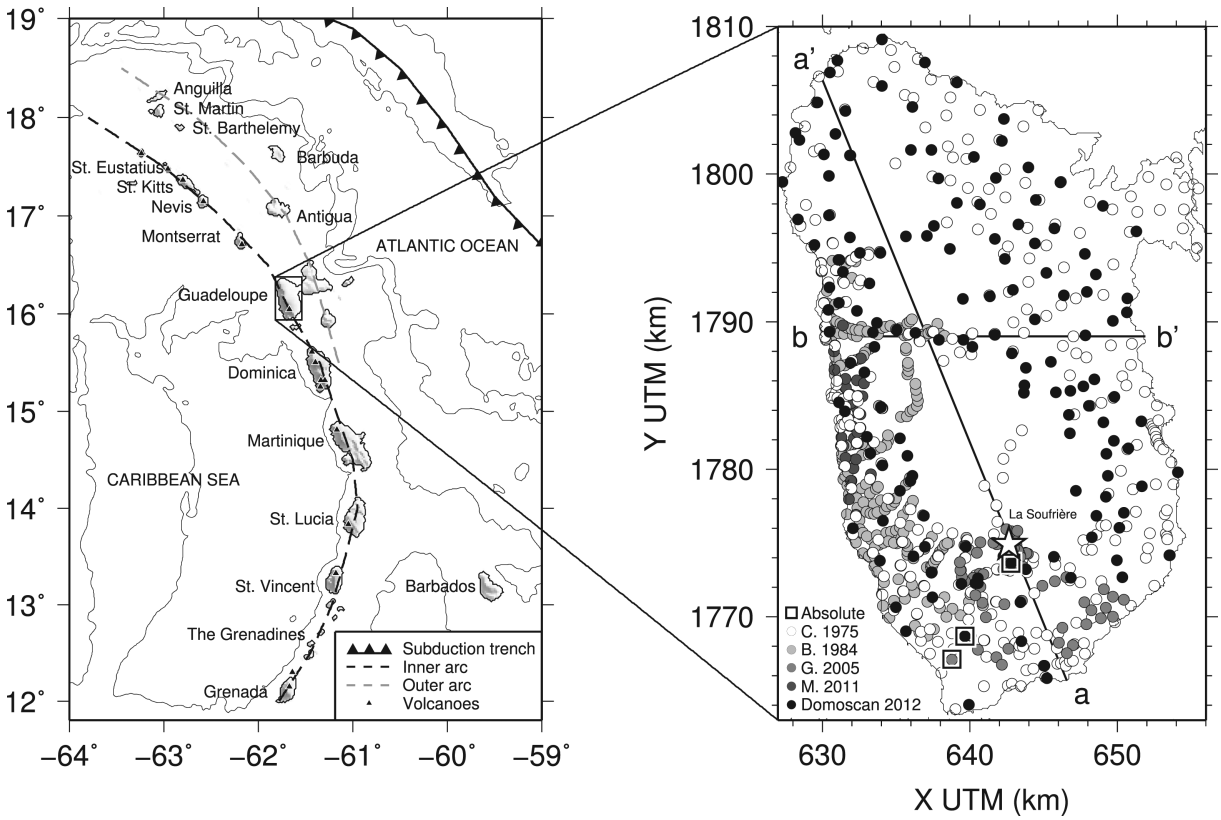

Figure 1. Left: Lesser Antilles map with bathymetry and shaded topography. Inner and outer arcs from Bouysse *et al.* (1988). Right: Basse-Terre island, Guadeloupe. Gravimetric data are indicated and sorted based on the first reference that used each data set—C. 1975 (Coron *et al.* 1975), B. 1984 (Barthes *et al.* 1984), G. 2005 (Gunawan 2005), M. 2011 (Matthieu *et al.* 2011) and Domoscan 2012 (new data from the 2012 campaign detailed in Section 4.2). Line aa′ (resp. bb′) shows the location of the sections of Fig. 3 (resp. Fig. 2). Squares indicate reference absolute gravity measurements (see Section 4.2).

This solution is appropriate when looking for particular structures such as dykes or layers.

In this paper, we adopt a Bayesian regularization approach combined with a grid node discretization of the space to linearly invert for 3-D density distributions. The Bayesian approach has also been used to introduce *a priori* knowledge on the density distribution (Boulanger & Chouteau 2001; Shamsipour *et al.* 2010) together with grid discretization (Marcotte *et al.* 2014). The parametrization of the problem and the inversion method are derived from seismological traveltime inversion techniques in order to facilitate joint inversion or comparison of density and seismic velocity models (e.g. Onizawa *et al.* 2002; Tiberi *et al.* 2003; Maceira & Ammon 2009). In particular, the formulation includes smoothing via explicit correlation functions that control the wavelengths of the recovered features and allow for multi-scale interpretation of the non-unique problem. The purpose of this paper is twofold. First, we detail and improve the approach for the inversion of gravity data that was used by Coutant *et al.* (2012) in a joint inversion scheme of seismic traveltime and gravimetric data. Second, we show that the methodology is useful for the inversion of gravity data alone using both synthetic and real data sets from the volcanic island of Basse-Terre in Guadeloupe.

The Guadeloupe archipelago is located in the Lesser Antilles arc resulting from the subduction of the Atlantic oceanic lithosphere beneath the Caribbean plate (Fig. 1, left). Basse-Terre is the main volcanic island of Guadeloupe and hosts the Soufrière active volcano, whose last magmatic eruption is dated around 1530 A.D. (Boudon *et al.* 2008). Since then, five series of phreatic eruptions occurred with the last one in 1976–1977 (e.g. Komorowski *et al.* 2005). Despite the numerous geological and geophysical studies performed on Basse-Terre island (e.g. Coron *et al.* 1975; Dorel *et al.* 1979; Brombach *et al.* 2000; Feuillet *et al.* 2002; Komorowski *et al.* 2005; Samper *et al.* 2007; Gailler *et al.* 2013; Mathieu *et al.* 2013), very few of these studies brought constraints on the structure of the island at depth and no 3-D density model has yet been published. Our inverse methodology is well-designed to overcome difficulties associated to the rugged topography of the island, the 3-D geometry of structures at depth, and the uneven distribution of data with measurement errors (Fig. 1, right). Before applying the methodology to the volcanic island of Basse-Terre, we designed synthetic data sets sharing similar characteristics with the real gravimetric data set of Basse-Terre in order to assess the advantages and limitations of the approach.

The paper is organized as follows: the second section details the gravity inversion methodology we use, the third section shows tests of the inversion on synthetic data sets and the fourth section presents the inversion of real data from the volcanic island of Basse-Terre and discusses the results with respect to the local geology and other geophysical studies.

2 METHODOLOGY

2.1 Formulation of the problem

Our objective is to invert for a 3-D heterogeneous distribution of density in a volume V given the observed vertical gravity field. As detailed in Section 2.2, the density $\boldsymbol{\rho}$ is discretized at nodes in the

volume V and is related to the produced gravimetric field $\boldsymbol{g}$ by the linear expression:

$$\boldsymbol{g} = \mathbf{G}\boldsymbol{\rho} \tag{1}$$

where $\mathbf{G}$ is the sensitivity kernel matrix.

Since we observe the gravity field resulting from the whole rotating Earth, we need to isolate the contribution of local density heterogeneities. To do so, corrections are traditionally applied to gravity observations to obtain the residual Bouguer anomaly $\Delta\boldsymbol{g}_{\text{res}}$ expressed here using notations similar to Blakely (1995):

$$\Delta\boldsymbol{g}_{\text{res}} = \boldsymbol{g}_{\text{obs}} - \boldsymbol{g}_0 - \boldsymbol{g}_{\text{fa}} - \boldsymbol{g}_{\text{b}} - \boldsymbol{g}_{\text{reg}} \tag{2}$$

where $\boldsymbol{g}_{\text{obs}}$ is the observed gravity, $\boldsymbol{g}_0$ the theoretical gravity field predicted for a reference geodetic system, $\boldsymbol{g}_{\text{fa}}$ the free air correction accounting for the variations of distance from the reference ellipsoid, $\boldsymbol{g}_{\text{b}}$ the Bouguer correction that corrects for the presence or absence of water and land masses compared to the reference ellipsoid, and $\boldsymbol{g}_{\text{reg}}$ the estimated regional field. The Bouguer correction is computed using a density for land masses, noted $\boldsymbol{\rho}_{\text{prior}}$. The residual Bouguer anomaly $\Delta\boldsymbol{g}_{\text{res}}$ thus reflects the effect of local density variations in V with respect to a reference density $\boldsymbol{\rho}_{\text{prior}}$.

The regional field $\boldsymbol{g}_{\text{reg}}$ is a qualitative estimation of the effect of remote sources outside the volume V and is thus composed of long-wavelength signals. It is usually estimated by fitting a bilinear or polynomial trend (e.g. Dentith & Mudge 2014). Here, we assume instead a constant value for the regional field $\boldsymbol{g}_{\text{reg}}$. Since we are able to perform inversions at different wavelengths, we split the inversion process in two steps: a long-wavelength inversion that will account for regional field variations,

$$\Delta\boldsymbol{g}_{\text{res}} = \mathbf{G}(\boldsymbol{\rho}_{\text{long}} - \boldsymbol{\rho}_{\text{prior}}) \tag{3}$$

and a short-wavelength inversion that will account for density heterogeneities in V,

$$\Delta\boldsymbol{g}_{\text{res}} - \mathbf{G}(\boldsymbol{\rho}_{\text{long}} - \boldsymbol{\rho}_{\text{prior}}) = \mathbf{G}(\boldsymbol{\rho}_{\text{short}} - \boldsymbol{\rho}_{\text{prior}}). \tag{4}$$

The following Section 2.2 details the computation of the sensitivity kernel $\mathbf{G}$ defined in eq. (1) as well as the Bouguer corrections $\boldsymbol{g}_{\text{b}}$ that appears in eq. (2).

2.2 Gravity modelling

We detail here the computation of the contribution of densities inside and outside the volume V to the gravity field. Our motivation is to use a model description and discretization that is compatible with a seismic velocity model and can easily be used either for direct comparison or for joint gravity and seismic inversion.

The volume V that we invert is a rectangular parallelepiped where density is given at $n_x * n_y * n_z$ nodes spaced by a constant step Δx. In the case of a joint inversion, the volume V is identical in size and node discretization for both density and velocity models. This volume is surrounded by a layered medium with vertical density gradients. The model is upper bounded by the topography which is taken into account with an arbitrary constant grid step δx.

The vertical gravitational field at point i is computed by integration over vertical prisms Ω_k of width $\Delta\Omega$, centred in (x_k, y_k) where $\delta x \leq \Delta\Omega \leq \Delta x$. This integration is performed numerically with respect to (x, y) assuming no lateral variation of density inside the prism, and analytically with respect to z. We assume linear variations of the density $\rho(z) = a + bz$ where a and b are linear combination of node densities in volume V and of layer densities outside volume V:

$$g(x_i, y_i, z_i) = \Delta\Omega^2\mathcal{G}\sum_{\Omega_k}\int_{z_a}^{z_b}\frac{\rho(x_k, y_k, z)(z_i - z)\mathrm{d}z}{((x_k - x_i)^2 + (y_k - y_i)^2 + (z - z_i)^2)^{3/2}} \tag{5}$$

where $\mathcal{G}$ is the gravitational constant. The topography is taken into account with its δx grid step in the vicinity of the gravity measurements and averaged over $\Delta\Omega \geq \delta x$ farther away.

This approach is similar to Banerjee & Gupta (1977) or García-Abdeslem & Martín-Atienza (2001) except that it can take into account linear variations of density. The validity of our code is tested following the strategy proposed by García-Abdeslem & Martín-Atienza (2001). We numerically compute the gravity field at the apex of a cone of constant density whose analytical solution is given by Tsuboi (1983). For a 1000 m width and 45° slope cone, we obtain absolute errors of 0.003, 0.003, 0.006 and 0.01 mGal with prism widths of 5, 10, 20 and 40 m, respectively. According to this test, a small enough prism width will guarantee a relative error smaller than 1 per cent. The precision is similar to those obtained by García-Abdeslem & Martín-Atienza (2001).

The Bouguer correction term g_b is computed by mean of eq. (5) using digital elevation models (DEMs) for topography and bathymetry, and prior density values for land and water as detailed in Section 4.2. Eq. (5) has linear contributions from the density nodes in volume V and from the surrounding layers. The sensitivity kernel $\mathbf{G}$ contains the contribution of the nodes to all observation locations.

2.3 Inversion methodology

The linear inverse problem $\boldsymbol{g} = \mathbf{G}\boldsymbol{\rho}$ (eq. 1) is well known to be non-unique, ill-conditioned and in our case, underdetermined (e.g. Aster *et al.* 2013). To solve the problem, we use the Bayesian approach of Tarantola & Valette (1982) and Tarantola (2005). We assume all *a priori* probability densities are Gaussian functions so that we can use the least-squares criterion to solve the problem in a deterministic way. We seek the density model $\widetilde{\boldsymbol{\rho}}$ that minimizes the objective function (Tarantola 2005):

$$\phi(\widetilde{\boldsymbol{\rho}}) = (\boldsymbol{g} - \mathbf{G}\widetilde{\boldsymbol{\rho}})^t\mathbf{C}_{\boldsymbol{g}}^{-1}(\boldsymbol{g} - \mathbf{G}\widetilde{\boldsymbol{\rho}}) + (\widetilde{\boldsymbol{\rho}} - \boldsymbol{\rho}_{\text{prior}})^t\mathbf{C}_{\boldsymbol{\rho}}^{-1}(\widetilde{\boldsymbol{\rho}} - \boldsymbol{\rho}_{\text{prior}}) \tag{6}$$

where $\boldsymbol{\rho}_{\text{prior}}$ is the *a priori* density model and $\mathbf{C}_{\boldsymbol{g}}$ and $\mathbf{C}_{\boldsymbol{\rho}}$ are the data and *a priori* model covariance matrices. The second term in the objective function (eq. 6) is a regularization term. It plays two roles: first it forces the solution to remain close to the prior model when it is not constrained by the data (controlled by the diagonal terms of $\mathbf{C}_{\boldsymbol{\rho}}$); second it forces the solution to be spatially correlated or smoothed (controlled by the off-diagonal terms of $\mathbf{C}_{\boldsymbol{\rho}}$).

The solution of the problem can be written as

$$\widetilde{\boldsymbol{\rho}} = \boldsymbol{\rho}_{\text{prior}} + \mathbf{C}_{\boldsymbol{\rho}}\mathbf{G}^t(\mathbf{G}\mathbf{C}_{\boldsymbol{\rho}}\mathbf{G}^t + \mathbf{C}_{\boldsymbol{g}})^{-1}(\boldsymbol{g} - \mathbf{G}\boldsymbol{\rho}_{\text{prior}}) \tag{7}$$

when the inverse problem is solved in the data space, or as

$$\widetilde{\boldsymbol{\rho}} = \boldsymbol{\rho}_{\text{prior}} + \left(\mathbf{G}^t\mathbf{C}_{\boldsymbol{g}}^{-1}\mathbf{G} + \mathbf{C}_{\boldsymbol{\rho}}^{-1}\right)^{-1}\mathbf{G}^t\mathbf{C}_{\boldsymbol{g}}^{-1}(\boldsymbol{g} - \mathbf{G}\boldsymbol{\rho}_{\text{prior}}) \tag{8}$$

for inversion in the model space (Tarantola 2005).

In a problem with n_g data and n_ρ parameters, $\mathbf{C}_{\boldsymbol{g}}$ and $\mathbf{C}_{\boldsymbol{\rho}}$ are square matrices of sizes $n_g * n_g$ and $n_\rho * n_\rho$ respectively. We assume that data are independent. The data covariance matrix $\mathbf{C}_{\boldsymbol{g}}$ is therefore diagonal and its diagonal of data variances $\boldsymbol{\sigma}_{\boldsymbol{g}}^2$ is based on estimated errors on the input data. The model covariance matrix $\mathbf{C}_{\boldsymbol{\rho}}$

is a full matrix that includes a variance on density as well as a spatial correlation function, or covariance function, used to smooth the result. This approach is particularly suitable in case studies where very little prior information is available (geological or geophysical constraints). Using a correlation function f_λ, the matrix element ij is written $\mathbf{C}_{\boldsymbol{\rho},ij} = \sigma^2_{\boldsymbol{\rho}} f_\lambda(D_{ij})$ where D_{ij} is the distance between model parameters i and j and λ is the spatial correlation length. We use here a Gaussian correlation function $f_\lambda(D_{ij}) = \exp(-\frac{D^2_{ij}}{\lambda^2})$ which leads to smoother models than when using an exponential function. The choice of the correlation length λ constrains the depth and minimum size of the structures that can be recovered by the inversion process. Therefore, inversions with different correlation lengths produce density models at different wavelengths, or scales. No trade-off factor is applied between the data and model terms of the objective function since the relative importance of the two terms can be adjusted by tuning the $\sigma_{\boldsymbol{\rho}}$ parameter until realistic densities are obtained in the resulting model.

Depending on the problem and on the size of the model and data spaces, it may be easier to solve the problem in the data space (eq. 7) or in the model space (eq. 8). We invert for n_ρ model parameters from n_g gravity data, with $n_g \ll n_\rho$. We recall that the sensitivity kernel $\mathbf{G}$ in gravimetry is a full $n_g * n_\rho$ matrix. Within the data space formulation (eq. 7), the largest matrix to compute is the full $n_\rho * n_\rho$ matrix $\mathbf{C}_{\boldsymbol{\rho}}$ but we only need to store the full $n_\rho * n_g$ matrix product $\mathbf{C}_{\boldsymbol{\rho}}\mathbf{G}^t$. This formulation requires solving a linear system of n_g equations. Within the model space formulation (eq. 8), covariance matrices appear in their inverse forms where $\mathbf{C}^{-1}_{\boldsymbol{\rho}}$ is a sparse matrix that can be estimated directly (Oliver 1998; Monteiller 2005; Coutant *et al.* 2012). The largest full matrix to store is therefore $\mathbf{G}$ of size $n_\rho * n_g$. Using this formulation, a linear system of n_ρ equations needs to be solved. In our gravimetric problem (with moderate n_ρ and $n_g \ll n_\rho$), we use here the data space formulation (eq. 7) because less equations need to be resolved. Note that one could also favour the model space formulation (eq. 8) to avoid the computation of the full model covariance matrix.

2.4 Resolution

Resolution indicates to which extent the solution is meaningful, yet it is rarely analysed in the inversion of potential fields (An 2012). The resolution matrix $\mathbf{R}$ relates the estimated parameters $\widetilde{\boldsymbol{\rho}}$ and the real parameters $\boldsymbol{\rho}_{\text{true}}$ (Menke 1989; Tarantola 2005):

$$(\widetilde{\boldsymbol{\rho}} - \boldsymbol{\rho}_{\text{prior}}) = \mathbf{R}(\boldsymbol{\rho}_{\text{true}} - \boldsymbol{\rho}_{\text{prior}}). \tag{9}$$

The resolution matrix $\mathbf{R}$ can be seen as the filter between the true model and the recovered model (Backus & Gilbert 1968; Tarantola 2005). A column gives the spreading of a parameter on its surrounding parameters while a row of the resolution matrix gives the linear dependency of the corresponding parameter to all of the other parameters of the model (e.g. Trampert *et al.* 2013). Backus & Gilbert (1968) introduced the concept of averaging kernel: appropriate elements extracted from the rows of the resolution matrix form bell-shaped curves (Backus & Gilbert 1968; An 2012) whose widths indicate the resolution lengths. However, $\mathbf{R}$ is an $n_\rho * n_\rho$ matrix expensive to compute and store. In seismic tomography, checkerboard and spike tests are commonly used to avoid expensive computations, but they can be misinterpreted (Lévêque *et al.* 1993; Trampert *et al.* 2013). One can prefer to compute and store only some meaningful resolution information for each model parameter. Some authors advocate the use of stochastic methods to efficiently estimate characteristics of the resolution matrix such as diagonals or spatial resolution lengths that quantify the size of the smallest recovered features (e.g. MacCarthy *et al.* 2011; An 2012; Trampert *et al.* 2013).

Our development allows to estimate spatial resolution lengths of the inverted models with a reasonable computational cost. In a Bayesian framework, each resulting model is an estimation of the densities with their a posteriori covariances $\widetilde{\mathbf{C}}_{\boldsymbol{\rho}}$ (Tarantola 2005):

$$\widetilde{\mathbf{C}}_{\boldsymbol{\rho}} = \mathbf{C}_{\boldsymbol{\rho}} - \mathbf{C}_{\boldsymbol{\rho}}\mathbf{G}^t(\mathbf{G}\mathbf{C}_{\boldsymbol{\rho}}\mathbf{G}^t + \mathbf{C}_{\boldsymbol{g}})^{-1}\mathbf{G}\mathbf{C}_{\boldsymbol{\rho}}. \tag{10}$$

While the *a priori* model covariance only depends on the chosen density distribution (density variance and smoothing), the a posteriori model covariance matrix also includes constraints from the geometry of the problem (contained in the sensitivity kernel $\mathbf{G}$ itself) and from the *a priori* error on the data. The explicit formulation of the resolution matrix with the Bayesian formalism is (Tarantola 2005):

$$\mathbf{R} = \mathbf{I} - \widetilde{\mathbf{C}}_{\boldsymbol{\rho}}\mathbf{C}^{-1}_{\boldsymbol{\rho}} = \mathbf{C}_{\boldsymbol{\rho}}\mathbf{G}^t(\mathbf{G}\mathbf{C}_{\boldsymbol{\rho}}\mathbf{G}^t + \mathbf{C}_{\boldsymbol{g}})^{-1}\mathbf{G}. \tag{11}$$

Here, we choose to estimate vertical and lateral resolution lengths following Backus & Gilbert (1968). For each node i of coordinates (x_i, y_i, z_i), we use the resolution parameters $r_i(x, y, z)$ between node i and nodes of coordinates (x, y, z) from the ith row of the resolution matrix $\mathbf{R}$. We numerically estimate the vertical resolution length L_z defined as:

$$L_z(x_i, y_i, z_i) = \frac{2\int |z - z_i||r_i(x_i, y_i, z)|\mathrm{d}z}{\int |r_i(x_i, y_i, z)|\mathrm{d}z}. \tag{12}$$

Resolution lengths L_x and L_y along the horizontal axes can be computed similarly. We rather compute a lateral resolution length L_{xy} defined as:

$$L_{xy}(x_i, y_i, z_i) = \frac{2\int s\overline{|r_i|}(s, z_i)\mathrm{d}s}{\int \overline{|r_i|}(s, z_i)\mathrm{d}s} \tag{13}$$

where $\overline{|r_i|}(s, z_i)$ is the average value of $|r_i|$ for nodes situated at the same distance s from node i on the horizontal plane $z = z_i$. In the end, we only store the estimated vertical and lateral resolution lengths for all density nodes. Fig. 2 illustrates the computation of resolution lengths L_x and L_z, along one horizontal axis for simplicity (Fig. 2b) and along the vertical axis (Fig. 2c), for density nodes at various depths. The example is based on the acquisition geometry and topography of Basse-Terre island (see Fig. 1 for data locations) and corresponds to an inversion with a correlation length of 4 km. As expected from the sensitivity kernel $\mathbf{G}$, we observe on Figs 2(b) and (c) that resolution decreases rapidly with depth, that is, resolution lengths increase with depth. In addition, vertical resolution lengths increase faster than lateral resolution lengths. This illustrates the fact that gravimetric inversions better constrain horizontal locations than vertical positions at depth.

3 TESTS ON SYNTHETIC DATA

We perform a series of 3-D synthetic tests in order to demonstrate the potential and limitations of the methodology and assess the results of Basse-Terre data inversion (part 4). We use the same 3-D configuration (topography, data distribution) as the real data. We compute the gravity data for four density models (Fig. 3a): (A) a thin shallow layer, (B) a thick deep layer, (C) a small shallow spherical body above a thick deep layer and (D) a thick deep layer beneath a thin shallow layer. A white noise with 1 per cent relative standard deviation is added to all gravity data. All models are inverted using a constant node spacing of 500 m, a constant ratio

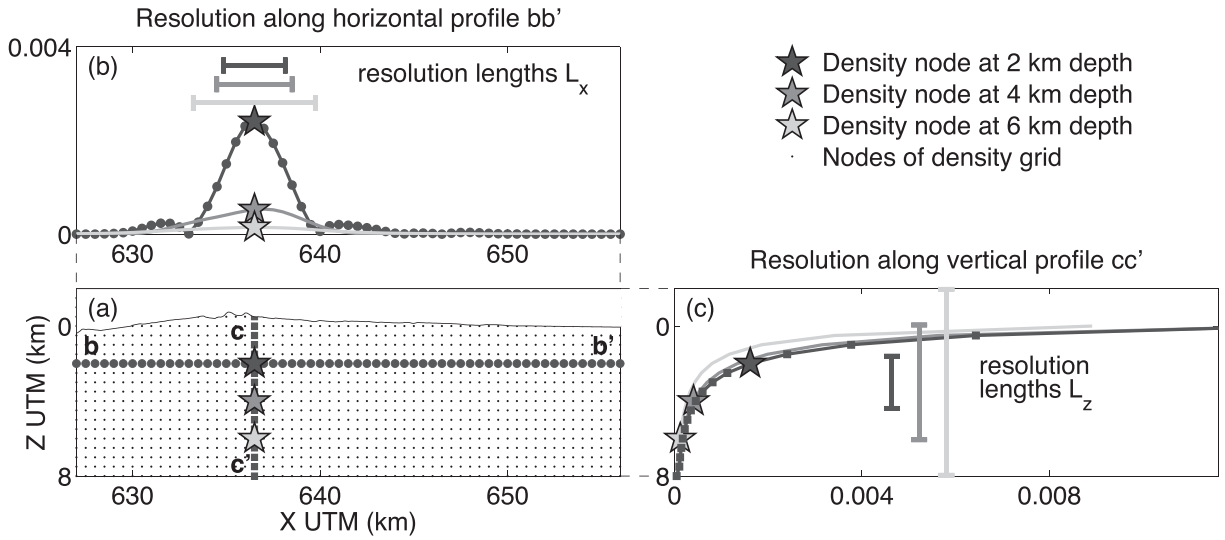

Figure 2. Resolution lengths for a 4 km correlation length inversion and density nodes at 2, 4 and 6 km depth. (a) Sketch of the node discretization along profile bb' (see Fig. 1). (b) Resolution along the x-axis and resolution lengths L_x for density nodes at 2, 4 and 6 km depth. (c) Resolution along the z-axis and resolution lengths L_z for density nodes at 2, 4 and 6 km depth. Axes of panels (a)–(c) share the same kilometre and resolution scales.

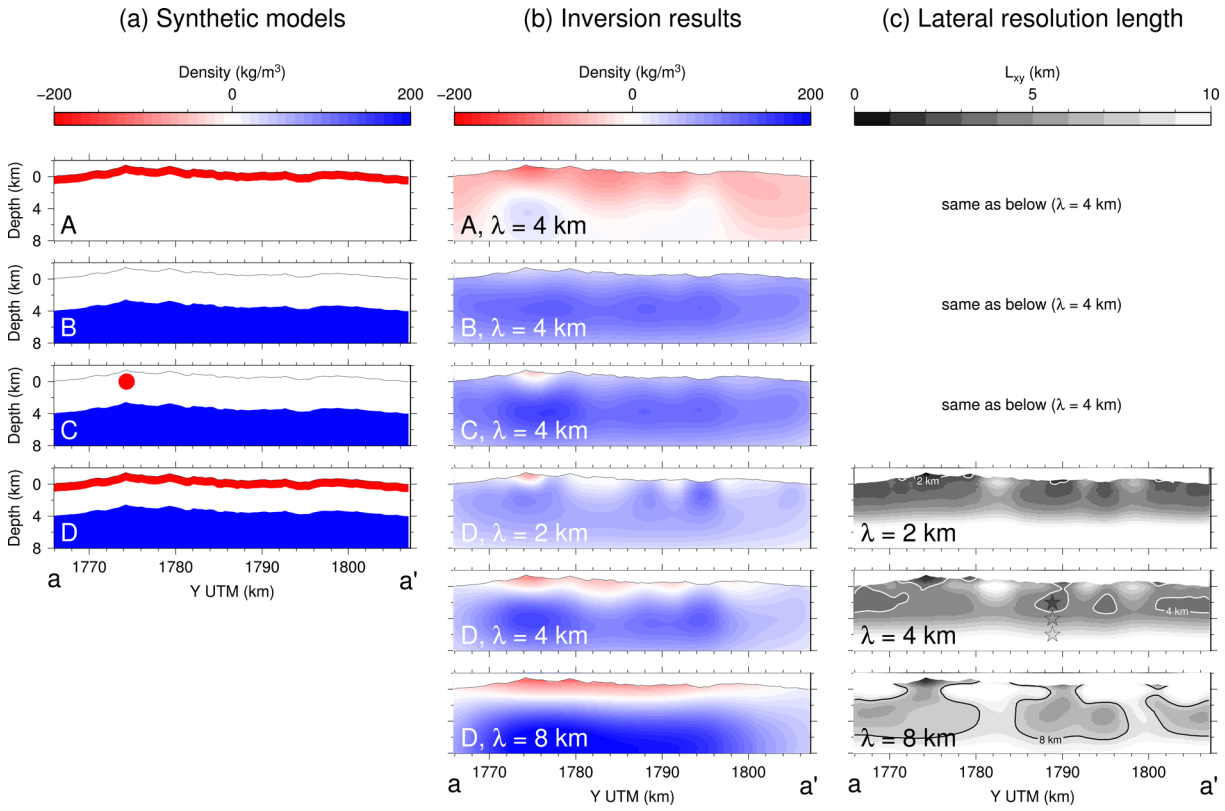

Figure 3. Section of 3-D inversions for synthetic models A, B, C and D. (see Fig. 1 for data disposition and location of section aa′). (a) Synthetic density models. (b) Density models resulting from the inversions with correlation lengths λ. (c) Lateral resolution lengths L_{xy} for correlation lengths λ.

$\sigma_{\boldsymbol{\rho}}/\sigma_{\boldsymbol{g}}$ of 50 kg m^{-3} mGal^{-1} and a correlation length of 2, 4 or 8 km (Fig. 3b). Lateral resolution lengths L_{xy} for inversions with correlation lengths of 2, 4 and 8 km are displayed on Fig. 3(c). Contours on Fig. 3(c) show where the densities are well resolved by the data (predominance of the first term in eq. 6).

The inversions of single layer models (A and B) performed with correlation length of 4 km, yield density anomalies that spread over the entire volume and are maximum at the surface for A, and around 4 km depth for B (Fig. 3b). In both cases, density amplitudes are smaller than original values due to this spreading. The thin shallow layer of model A cannot be recovered due to grid spacing and correlation length, the inversion gives high relative RMS of data residuals (Table 1).

Results for model D (Fig. 3b) and plots of lateral resolution length L_{xy} (Fig. 3c) show how the correlation length affects the inversion results. Increasing the correlation length λ induces larger resolution length L_{xy} at shallow layer, and smaller resolution length at depth. Thus, larger λ values favour resolution at larger depth and move

Table 1. Amplitude of data variations and RMS of data residuals for the synthetic tests (Fig. 3). RMS are given both in mGal and in percentage of the amplitude of the synthetic data variations.

Model	Data amplitude	Correlation length	RMS of data residuals
A	5.02 mGal	4 km	0.30 mGal (6.0 per cent)
B	11.85 mGal	4 km	0.14 mGal (1.2 per cent)
C	11.78 mGal	4 km	0.19 mGal (1.6 per cent)
D	11.66 mGal	2 km	0.34 mGal (3.0 per cent)
D	11.66 mGal	4 km	0.36 mGal (3.1 per cent)
D	11.66 mGal	8 km	0.37 mGal (3.2 per cent)

anomalies deeper, with increasing size. The use of various smoothing correlation length can therefore be seen as an alternative to Li & Oldenburg (1998) depth weighting to counteract the decrease of sensitivity with depth. On the other end, for short correlation lengths, the anomalies are concentrated where resolution is higher (small L_{xy} length), that is, towards the surface and below areas with good data coverage. As a result, lateral variations of density in the 2 km correlation length inversion of model D might be misinterpreted with the presence of anomalous bodies, as in model C, instead of continuous layers. Increasing the correlation length allows to distinguish between layers and bodies: inversion of model D at 4 km is no longer similar to inversion of model C. Finally, RMS of data residuals increases with the correlation length (Table 1) since we add more constraints to regularize the inversion. Contours on Fig. 3(c) delineate where data allow to resolve structures smaller than the correlation length. The minimum correlation length to be used can be inferred from the minimum resolution length. Here L_{xy} is always larger than 2 km, so smaller λ values would not bring any additional information.

These synthetic tests show, as expected, that the inversion produces smooth density models and does not recover sharp discontinuities or thin layers. However, inversions at different correlation lengths outline the evolution of the model with scale and avoid misinterpreting the recovered features. We therefore advocate the use of multi-scale inversions to better interpret the resulting models with respect to the intrinsic non uniqueness of gravity inversions. It is worth noting that this approach shares some ideas with wavelet decomposition applied in potential field studies (e.g. Sailhac & Gibert 2003). Finally, resolution analysis is necessary to understand the effect of the distribution of data and of the spatial correlation length on the inverted densities.

4 APPLICATION TO BASSE-TERRE, GUADELOUPE, LESSER ANTILLES

4.1 Geological context and previous geophysical studies

The Lesser Antilles subduction arc includes an inner arc composed of active volcanic islands and an outer arc corresponding to former volcanic islands now covered by sediments (Fig. 1). The Guadeloupe archipelago overlaps the two arcs. Basse-Terre is the main volcanic island of Guadeloupe and is part the inner arc. This island displays several eruptive fields, each containing several eruptive centres that form a continuous chain trending NNW–SSE (see Fig. 4). A southward migration of volcanism is observed across geological times, forming, in the chronological order (ages from Carlut *et al.* 2000; Feuillet *et al.* 2002; Samper *et al.* 2007; Lahitte *et al.* 2012): the Basal Complex (2.79–2.68 Myr), the Septentrional Chain (1.81–1.15 Myr), the Axial Chain, Sans-Toucher and Bouillante Chain (1.02–0.435 Myr), the Monts Caraïbes (555–472 kyr), the Itacques–Capesterre and Vieux-Habitants volcanics (600–200 kyr),

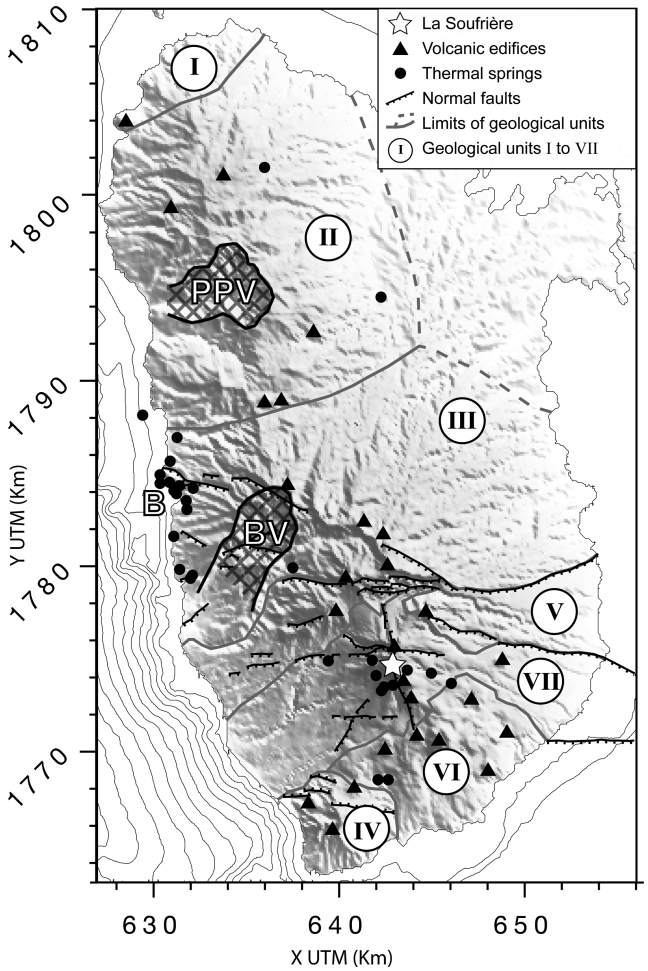

Figure 4. Main geological features of the island of Basse-Terre after Bézèlgues-Courtade & Bes-De-Berc (2007), Brombach *et al.* (2000), Feuillet *et al.* (2002), Komorowski *et al.* (2005), Mathieu *et al.* (2011, 2013) and Samper *et al.* (2007). Geological units numbered in chronological order: I, Basal Complex; II, Septentrional Chain; III, Axial Chain, Sans-Toucher and Bouillante Chain; IV, Monts Caraïbes; V, Icaques-Capesterre and Vieux-Habitants volcanics; VI, Madeleine vents and Trois-Rivières Complex; VII, Grande-Découverte Carmichaël Complex and Soufrière Complex. Other places mentioned in the article: B, Bouillante; PPV, Petite Plaine Valley; BV, Beaugendre Valley.

the Madeleine vents and Trois Rivière Complex (150–11 kyr) and the Grande-Découverte Carmichaël Complex and Soufrière Complex (200 kyr-present) that hosts the active Soufrière of Guadeloupe active volcano (Fig. 4). These volcanic fields include mainly lava flows and domes of andesitic to basaltic-andesitic composition but also scoria domes and pyroclastic deposits and acidic rocks of dacitic or rhyolitic composition. The northeastern part of the

island is covered by sediments. Fig. 4 also displays the main known tectonic features such as faults and flank collapse scars. Note that the higher density of mapped structures in the recent southern part of Basse-Terre might simply reflect the larger number of studies focusing in this area and difficulties to map structures that have been eroded or covered by sediments in the north. Intense hydrothermal activity is currently observed in the Bouillante geothermal area and within the Soufrière volcano (see the location of thermal springs in Fig. 4).

Very few geophysical studies have been performed at the scale of the island of Basse-Terre, while many surveys have been conducted at the scale of the dome of the Soufrière of Guadeloupe volcano. Geophysical works at the scale of the dome focused on an area of 2×2 km^2 at most using various methods: electrical resistivity imaging (Zlotnicki & Nishida 2003; Nicollin *et al.* 2006; Zlotnicki *et al.* 2006; Lesparre *et al.* 2014), seismic velocity imaging (Coutant *et al.* 2012) and density imaging (Coutant *et al.* 2012; Lesparre *et al.* 2012). Coutant *et al.* (2012) produced 3-D velocity and density models of the dome by joint inversion of active seismic and gravimetric data. These studies aimed to provide a better understanding of the structure and activity of the superficial hydrothermal system. Some other local studies were performed in the area of Bouillante for geothermal exploration purposes (Barthes *et al.* 1984; Debeglia *et al.* 2007; Matthieu *et al.* 2011; Gailler *et al.* 2014). At the scale of the island of Basse-Terre (30×40 km^2 approximately), geophysical surveys were used for either qualitative interpretation of local anomalies or inversions along 2-D profiles. Aeromagnetic data were acquired in 1975 (Le Borgne & Le Mouël 1976; Le Mouël *et al.* 1979). Three active seismic profiles were shot across the island (Dorel *et al.* 1979). Several sets of gravimetric data were analyzed: Coron *et al.* (1975) provided a gravimetric database over all the islands of the Guadeloupe archipelago, Gunawan (2005) focused on the south of Basse-Terre corresponding to the most recent volcanic complex. Gailler *et al.* (2013) compiled gravimetric and magnetic data sets from previous land and marine surveys to produce maps of the Bouguer anomaly and of the reduced to the pole magnetic anomaly. The authors constructed 2-D vertical layered models of densities and magnetizations along profiles based on the 2-D seismic velocity structures provided by Dorel *et al.* (1979). However, volcanic structures are highly heterogeneous media and 2-D models do not account for multi-dimensional variations. No geophysical study has yet led to a 3-D model of the whole island of Basse-Terre. In the followings, the methodology developed in part 2 is applied to gravimetric data sets from Basse-Terre to produce 3-D density models of the island.

4.2 Data and processing

The methodology is applied to a composite data set of gravimetric data from the island of Basse-Terre in Guadeloupe. We compiled land data from previous studies (Coron *et al.* 1975; Barthes *et al.* 1984; Gunawan 2005; Matthieu *et al.* 2011) and acquired new data in 2012 within the frame of the Domoscan ANR project (see Fig. 1). The scope of the 2012 gravimetric campaign was to provide data covering the whole island of Basse-Terre with high precision measurements and localizations which are necessary for the inversion. The data were acquired with two Scintrex CG5 relative gravimeters and localized using differential GPS. A tide correction is applied using the Longman (1959) formula implemented in the Scintrex CG5 gravimeters. We then correct these relative measurements for instrumental drift and convert them to absolute values based on absolute measurements performed with a Micro-g LaCoste A10 gravimeter at three locations close to the Soufrière of Guadeloupe volcano: at the Observatoire Volcanologique et Sismologique de Guadeloupe on the Houëlmont, in front of the church of Gourbeyre and on the parking of the Savane-à-Mulets (see localizations on Fig. 1). Note that the reference used for absolute values does not impact the inversion results as only amplitude variations matter. Finally, the four other data sets were adjusted with our measurements by comparing collocated gravity values.

Altitudes of all measurements are compared with a 1 m resolution Lidar DEM available for the whole island (Litto3D data). For the data acquired in 2012, we estimate the error on altitudes from differential GPS to 17 cm. The difference between these GPS altitudes and their projections on the DEM indicates a standard error for DEM altitudes of 28 cm. We use all the data from the 2012 campaign and from Matthieu *et al.* (2011) as the comparison with the DEM shows accurate localizations. We discard data from the three previous data sets (Coron *et al.* 1975; Barthes *et al.* 1984; Gunawan 2005) when the difference between the provided altitude and the projection onto the DEM is greater than the median plus or minus half of the standard deviation of the altitude differences. We then estimate the standard errors for the remaining altitudes from the previous data sets: 35 cm (Matthieu *et al.* 2011), 1.94 m (Gunawan 2005), 3.38 m (Barthes *et al.* 1984) and 4.42 m (Coron *et al.* 1975). We use the GPS altitudes for the data of the 2012 campaign and the Lidar DEM altitudes for anterior measurements whose altitudes are less accurate. In total, 999 values are used for the inversion: 338 from Coron *et al.* (1975), 323 from Barthes *et al.* (1984), 157 from Gunawan (2005), 37 from Matthieu *et al.* (2011) and 144 from the new measurement campaign. The full data set is then processed to compute the complete Bouguer anomalies as detailed in the next two paragraphs.

The theoretical gravity produced by the World Geodetic System 1984 (WGS84) is derived using the closed-form formula proposed by Somigliana in 1929 (Hofmann-Wellenhof & Moritz 2005). The free-air correction is computed up to the second order in terms of ellipsoidal height, following the recommendations of Li & Götze (2001) and Hackney & Featherstone (2003).

DEMs of various resolutions are used to take into account the topography and the bathymetry. We used: Litto3D data for the topography of Guadeloupe and its coastal bathymetry, bathymetry from the Aguadomar marine survey conducted in the central part of the Lesser Antilles arc (Deplus *et al.* 2001) and ETOPO1 bathymetry and topography elsewhere. Topography and bathymetry are taken into account with a resolution of 1 m up to a distance of 500 m away from the station when available. Farther away and up to 120 km, a resolution of 100 m is used. These parameters were adjusted by convergence analysis of the modelled gravity field. The ocean surface is considered with a resolution of 100 m based on the altimetric grid of the IGN in the Guadeloupe archipelago area and on the Earth Gravitational Model 2008 (Pavlis *et al.* 2008) further away. The Bouguer anomaly is computed assuming a density of 1026 kg m^{-3} for sea water (Wang *et al.* 2010) and a mean density of 2600 kg m^{-3} for land masses estimated via the Parasnis method (Parasnis 1972). Using the same method, Gunawan (2005) proposed a mean density of 2500 kg m^{-3} for the southern part of Basse-Terre, resulting from an average density of 2210 kg m^{-3} for the dome and of 2710 kg m^{-3} for the surrounding rocks. Coron *et al.* (1975) corrected their gravimetric data from the Guadeloupe archipelago with a density of 2670 kg m^{-3} except for the area of La Soufrière where they used a density of 2500 kg m^{-3}. Our mean value of 2600 kg m^{-3} for Basse-Terre island is in accordance with these density ranges. The average

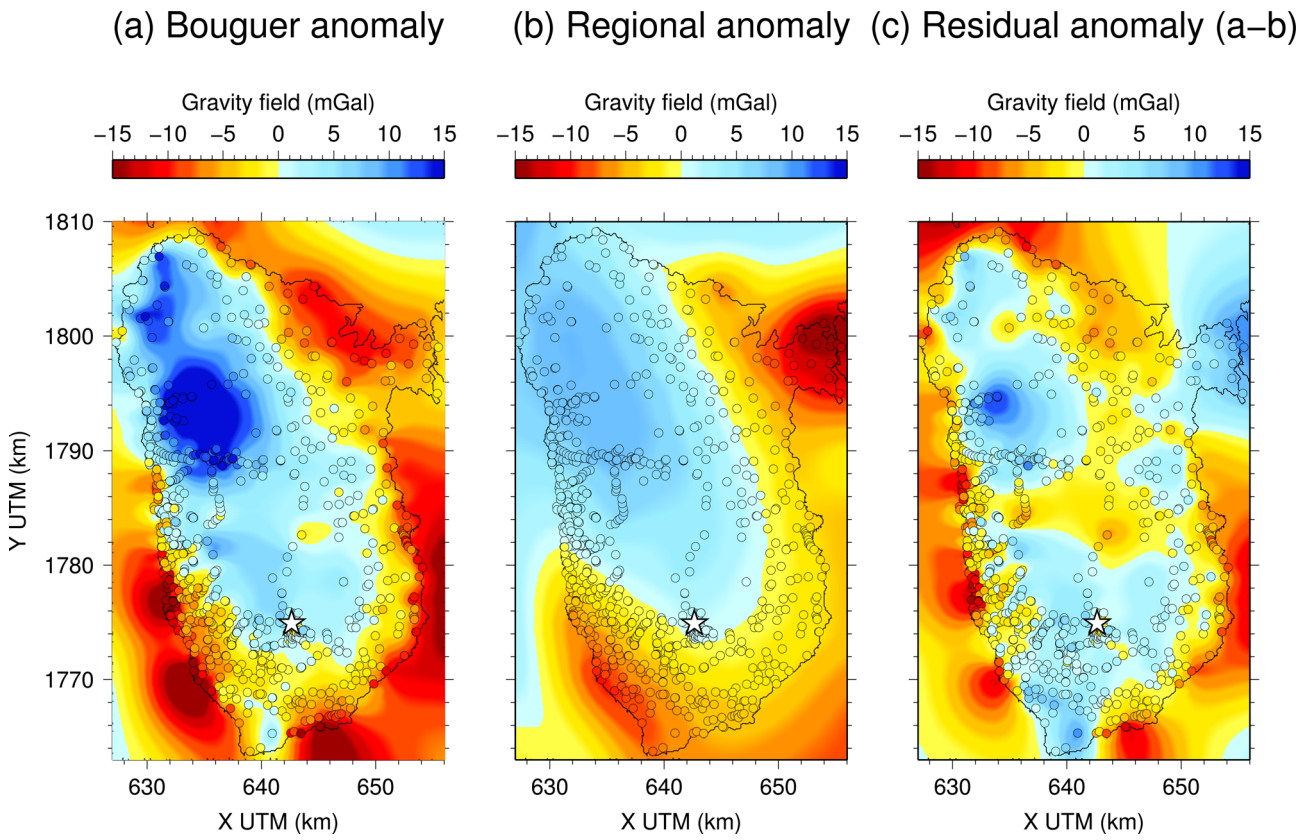

Figure 5. Gravity anomaly. Gridded data are represented along with the original data used as input and output for the inversions (filled circles). White star: La Soufrière. (a) Gravity anomaly used as input for the long-wavelength inversion ($\lambda = 80$ km) providing an estimation of the regional field. (b) Regional gravity anomaly deduced from the result of the long-wavelength inversion. (c) Residual gravity anomaly (a–b) used as input for the short-wavelength inversions.

value of the Bouguer anomaly is subtracted to obtain a zero-mean anomaly (Fig. 5a).

The Bouguer anomaly map represented on Fig. 5(a) shows long-wavelength and short-wavelength features. We globally observe negative anomalies near the coast and in the southern part and positive anomalies inland. Short-wavelength anomalies locally display some correlations with topography. This is obvious in the SW part of Basse-Terre near the Bouillante geothermal area (see Bouillante location on Fig. 4), where dense measurements are available. In this area, measurements acquired at high elevation (along the crests) provide negative anomalies whereas measurements acquired at low elevation (in valleys) provide positive anomalies. Such correlation with topography suggests that, in this area, the real density is different from the density that we used to compute the Bouguer anomaly.

Our Bouguer, regional and residual Bouguer anomaly maps (Figs 5a–c) are similar to the corresponding maps obtained by Coron *et al.* (1975) but include more details, mainly in the southeast part of Basse-Terre where dense surveys are now available (Barthes *et al.* 1984; Gunawan 2005). Compared to the residual Bouguer anomaly map presented by Gailler *et al.* (2013), our map contains only the shortest wavelengths needed for the inversion (Fig. 5c).

Errors on Bouguer anomalies are estimated step by step throughout the acquisition and processing as summarized in Table 2. Precision of gravity measurements (including errors on the estimation of instrumental drift) is evaluated by comparison of collocated acquisitions. Errors on latitude and free air corrections combine the numerical precision of formulas and the propagation of localization errors. Finally, we estimate errors on Bouguer corrections from localization errors and the numerical precision of the modelling code. Note however that Bouguer corrections are also affected by the DEM precision, which is not taken into account in the value displayed in Table 2. Highest uncertainties come from the precision of gravity measurements and from the propagation of elevation errors in the free air correction computation. The total error on processed data from the 2012 campaign is estimated to about 0.3 mGal. Gunawan (2005) estimated an error of 0.4 mGal for his data. We expect the data from Matthieu *et al.* (2011) to reach the same quality and assign them an error of 0.4 mGal as well. Errors on anterior data (Coron *et al.* 1975; Barthes *et al.* 1984) are significantly higher mostly due to higher uncertainties in their localizations so we use an error of 1 mGal, in accordance with the estimations of the authors.

Table 2. Summary of errors associated to data acquisition and processing.

Source of error	Error (mGal)
Measurements and drift correction	≤ 0.2
Latitude correction	≤ 0.01
Free air correction	0.08
Bouguer corrections	≤ 0.2
Total	**0.3**

To summarize, our new data set provides a good coverage of the island with precise estimations of the Bouguer anomaly with measurement errors estimated to about 1 per cent of the anomaly amplitude (Fig. 5a). Note however that the distribution

of data after merging the five data sets remains uneven with large gaps over inaccessible areas, mainly in the central part of the island (Fig. 1).

4.3 Inversion results

The inversion is performed using a 3-D grid that encompasses the whole island of Basse-Terre (boundaries are the limits of Fig. 5), down to 8 km depth. We use a grid node spacing of 500 m, approximately corresponding to the mean distance between gravimetric stations, which satisfies the criteria proposed by Boulanger & Chouteau (2001). The data are assigned a standard deviation of 0.3 mGal (newly acquired data), 0.4 mGal (Gunawan 2005; Matthieu *et al.* 2011) or 1 mGal (Coron *et al.* 1975; Barthes *et al.* 1984), as explained in Section 4.2. The *a priori* densities are centred on the value of 2600 kg m^{-3}, used for the Bouguer corrections, with a standard deviation set to 20 kg m^{-3}. This value is tuned to obtain realistic density ranges in the final models.

A preliminary inversion is performed using a long correlation length λ of 80 km in order to extract the regional gravity field variations from the data (Fig. 5b). The residual Bouguer anomaly (Fig. 5c) is then used as input for short-wavelength inversions. Fig. 6 shows vertical sections and maps extracted from the 3-D inversion results using correlation lengths of 2, 4, and 8 km. RMS of data residuals are given in Table 3. We observe that when the correlation length increases, anomalous bodies are recovered at larger depths and with larger wavelengths. The RMS of data residuals also becomes larger as we add constraints to the model. These behaviours have already been observed with the inversion of the synthetic model D (Section 3, Fig. 3 and Table 1).

4.4 Interpretation and discussion

We adjust the choice of standard deviation for the *a priori* density model in order to keep the density values in the range 2600 kg m^{-3} $\pm$ 200 kg m^{-3}. Rock sample density values obtained by Feuillard (1976), Bernard *et al.* (2014) and Gailler *et al.* (2014) range between 1500 and 2800 kg m^{-3} at surface or in shallow boreholes. The lowest densities were found for superficial material around the dome of La Soufrière or Bouillante hydrothermal systems. However, data resolution and the associated node discretization step (500 m) cannot reproduce shallow structures and 2400 kg m^{-3} is a reasonable lower bound value.

The structure of Basse-Terre island presents two key issues associated with La Soufrière active volcano: (i) the depth of the expected magmatic chamber and (ii) the extent of the hydrothermal system. For the first point, the superficial magma chamber is thought to lie around 6 km below sea level with an approximate radius of 1 km (e.g. Pozzi *et al.* 1979; Boichu *et al.* 2011; Allard *et al.* 2014). We cannot expect to find a signature of this chamber considering its size and our data distribution. We identify three main characteristics in our inversion results (Fig. 6): first, most of the anomalies are aligned along the NNW–SSE axis of volcanic edifices that form the island (see Figs 6a and 4) associated with generally decreasing densities southwards; second, three high density anomalies lie at depth (especially well distinguished on Fig. 6a, middle); third, shallow low-density material is present in the southern part of Basse-Terre. We discuss these features below.

The NNW–SSE alignment of density anomalies following the axis of volcanic edifices suggests heterogeneities in the volcanic material produced by the successive eruptive episodes. This trend is also consistent with the regional tectonic setting, as it is parallel to the Bouillante–Montserrat offshore active fault system (Bouysse *et al.* 1988). We also observe that density globally decreases southwards at the scale of Basse-Terre. The local geology is in accordance with this trend: based on geomorphological observations and geochemistry data, Mathieu *et al.* (2013) suggest an increase towards the south in the proportion of acidic and viscous volcanic rocks which have lower density than andesite and basaltic andesite. Our inversion also suggests that dense material compose the Basal Complex in the northwest (see location on Fig. 4), in agreement with the overall decreasing density southwards, and the Monts Caraïbes at the very south of the island. As for the northeast part of the island characterized by low gravity values, the inversion recovers low-density material corresponding to the sedimentary cover.

Low-density anomalies lie at shallow depths in the southern part of the island. The low-density zone is concentrated in the graben bounded to the north by the major fault at the south of the Axial Chain (Fig. 4), interpreted as the prolongation of the offshore Bouillante-Montserrat fault system (Bouysse *et al.* 1988; Feuillet *et al.* 2002, 2010). Low-density anomalies of high amplitude are well distinct in the inversion results as long as the lateral resolution length (Fig. 6b) is much shorter than the distance between the two anomalies (about 10 km). One is situated in the area of La Soufrière volcano and La Ty fault at shallow depths. It is a signature of the underlying hydrothermal system. This observation is consistent with the lower seismic wave velocities of the shallow layers in the area of the dome of the Soufrière volcano as outlined in the velocity models by Dorel *et al.* (1979) and in the low surface wave velocities determined by Collet (2010) in the vicinity of the dome. However, the precise extent of the hydrothermal system cannot be determined from gravity data alone. Other very low density anomalies are located near Piton de Bouillante edifice and along the western coast, reflecting high level of alteration. The low densities are therefore due to a combination of faulting, hydrothermal alteration, and deposition of debris flows (Brombach *et al.* 2000; Feuillet *et al.* 2002; Lahitte *et al.* 2012). Thermal springs across the island (Fig. 4) are well correlated with shallow low-density anomalies. In particular, the Bouillante Chain along the western coast is famous for geothermal exploration and exploitation (e.g. Gailler *et al.* 2014). The high-porosity of these structures explains the inferred low densities, similarly to the conclusion of Linde *et al.* (2014) in the case of the Stromboli volcano.

Three high-density anomalies are identified at depth beneath Petite Plaine Valley in the north, beneath Beaugendre Valley dominated by Piton de Bouillante and beneath the Grande-Découverte-Carmichaël-Soufrière Complex in the south (see locations on Fig. 4). This observation is consistent with the density of 2750 kg m^{-3} measured by Gailler *et al.* (2014) in massive lava flows in the Beaugendre area. Mathieu *et al.* (2013) outlined abundant lava flows in Petite Plaine Valley and Beaugendre Valley areas. The Grande-Découverte-Carmichaël-Soufrière Complex is the most recent volcanic complex of the island (e.g. Komorowski *et al.* 2005; Lahitte *et al.* 2012). The three dense anomalies could therefore correspond to major eruptive centres that were active in the past on Basse-Terre. Dense structures at depth in volcanic areas have been reported many times and interpreted as solidified intruded magma from earlier volcanic activity (e.g. Aoki *et al.* 2009; Camacho *et al.* 2009; Liuni *et al.* 2010; Aoki *et al.* 2013). The structures we identify might therefore correspond to the solidified superficial magma chamber of the associated eruptive centres.

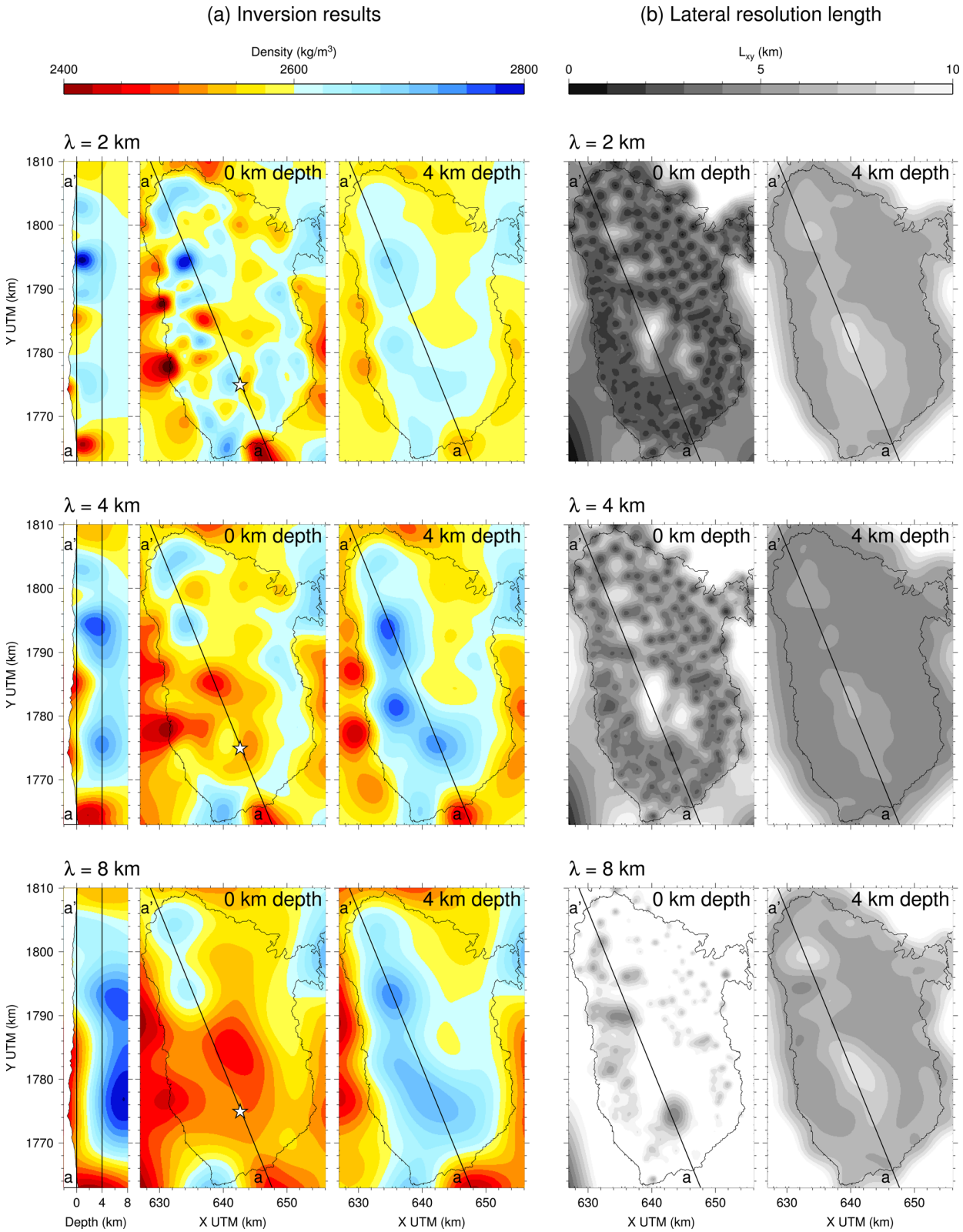

Figure 6. Results for inversions with correlation lengths λ of 2 km (top), 4 km (middle) and 8 km (bottom). (a) 2-D sections extracted from the 3-D density models. White star: La Soufrière. (b) Lateral resolution lengths L_{xy} for the horizontal sections.

Table 3. RMS of data residuals for the inversions of Bouguer anomalies with different spatial correlation lengths. RMS are given both in mGal and in percentage relative to the amplitude of the data variations (30 mGal).

Correlation length	RMS of data residuals
2 km	1.8 mGal (6.5 per cent)
4 km	1.9 mGal (7.1 per cent)
8 km	2.2 mGal (8.3 per cent)

5 CONCLUSIONS

We have followed the Bayesian approach of Tarantola & Valette (1982) combined with a grid node discretization of the space to linearly invert for 3-D density distribution. The method and discretization of the problem present the advantage to be compatible with seismic tomography to favour the comparison and joint inversion of density and velocity models. The forward modelling takes into account the topography and expresses the gravimetric field as a linear combination of node densities. The inverse methodology includes covariances matrices that force the solutions to be spatially correlated, hence smoothed. The choice of the correlation length constrains the minimum size of the structures that can be recovered. Our developments include the quantitative estimation of lateral and vertical resolution lengths with a reasonable computational cost and allow for resolution analysis that is rarely performed in the inversion of potential field data. A preliminary inversion with a large correlation length allows to isolate the large wavelength component of the gravity field, that is, the regional field. Short-wavelength inversions can then be performed and interpreted.

Tests on synthetic data were performed to show the potential and limitations of the methodology. We observed that spatial spreading of causative bodies prevents from properly recovering amplitudes of density variations. Node discretization and smoothing prevent from recovering structures such as a thin shallow layer. Synthetic models inverted with various correlation lengths outlined the advantages of the method as resolution at depth varies with the correlation length used in the inversion. Confronting results at different scales helps identifying anomalous structures to be interpreted. Resolution lengths allow to outline areas where features are better or less resolved depending on the data distribution and the correlation length.

We inverted gravimetric data of the volcanic island of Basse-Terre. We benefited from a new high quality data set (errors of about 1 per cent of the amplitude of gravity anomaly variations, 1 m resolution Litto3D DEM). Despite the dense data coverage in accessible areas, large parts remain uncovered inside the island. Our inversion approach provided smooth 3-D density models of the volcanic island of Basse-Terre at various scales to overcome difficulties associated to the uneven distribution of data and the few available geological or geophysical constraints. Results showed an obvious NNW–SSE trend with densities generally decreasing southwards and anomalies located along the axis of successive volcanic centres. These observations are consistent with the geological history of the island (e.g. Samper *et al.* 2007; Mathieu *et al.* 2013) and suggest that density anomalies reflect variations in the characteristics of different eruptive episodes. Dense anomalies beneath Petite Plaine Valley, Beaugendre Valley and the Grande-Découverte-Carmichaël-Soufrière Complex are interpreted as solidified magmatic intrusions from major eruptive centres. Shallow depth low-density anomalies are observed in the Soufrière and Piton de Bouillante areas and along the western coast and reflect the presence of hydrothermal systems and the high porosity of fractured and altered rocks. These first 3-D models of Basse-Terre bring new insights about the internal structure of the island. Further geological and geophysical studies would help comforting our interpretations.

ACKNOWLEDGEMENTS

We thank Michel Diament and an anonymous reviewer for their comments that greatly help improving the manuscript. We benefited from invaluable help from the staff of the 'Observatoire Volcanologique et Sismologique' de Guadeloupe (OVSG-IPGP) and we especially thank Michel Dietrich and Anna Pourchot for their help in the field. The gravimeters were provided by the French national pool of mobile gravimeters Gmob (CNRS-INSU). Financial supports were provided through ANR contracts CATEL/RISK-VOLCAN, RISK-2008/DOMOSCAN and CNRS-INSU PNRN program. The International Gravimetric Bureau (2012, http://bgi.obs-mip.fr, last accessed 8 February 2016) and the Bureau des Recherches Géologiques et Minières provided gravimetric data sets. The Litto3D data are provided by the Service hydrographique et océanographique de la marine (SHOM) and the Institut national de l'information géographique et forestière (IGN). Most of the computations presented in this paper were performed using the Froggy platform of the CIMENT infrastructure, which is supported by the Rhône-Alpes region (GRANT CPER07_13 CIRA) and the Equip@Meso project (ANR-10-EQPX-29-01) of the programme Investissements d'Avenir supervised by the Agence Nationale pour la Recherche. ISTerre is part of Labex OSUG@2020 (ANR10 LABX56).

REFERENCES

Allard, P. *et al.*, 2014. Steam and gas emission rate from La Soufrière volcano, Guadeloupe (Lesser Antilles): implications for the magmatic supply during degassing unrest, *Chem. Geol.,* **384,** 76–93.

An, M., 2012. A simple method for determining the spatial resolution of a general inverse problem, *Geophys. J. Int.,* **191,** 849–864.

Aoki, Y. *et al.*, 2009. P-wave velocity structure beneath Asama Volcano, Japan, inferred from active source seismic experiment, *J. Volcanol. Geotherm. Res.,* **187,** 272–277.

Aoki, Y., Takeo, M., Ohminato, T., Nagaoka, Y. & Nishida, K., 2013. Magma pathway and its structural controls of Asama Volcano, Japan, *Geol. Soc. Spec. Pub., London,* **380,** 67–84.

Aster, R.C., Borchers, B. & Thurber, C.H., 2013. *Parameter Estimation and Inverse Problem,* 2nd edn, Academic Press.

Backus, G.E. & Gilbert, J.F., 1968. The resolving power of gross Earth data, *Geophys. J. R. astr. Soc.,* **16,** 169–205.

Banerjee, B. & Gupta, S.P.D., 1977. Gravitational attraction of a rectangular parallelepiped, *Geophysics,* **42**(5), 1053–1055.

Barbosa, V. C.F. & Silva, J.B.C., 1994. Generalized compact gravity inversion, *Geophysics,* **59**(1), 57–68.

Barthes, V., Mennechet, C. & Honegger, J.L., 1984. Prospection géothermique, La région de Bouillante - Vieux Habitants, Guadeloupe: Étude gravimétrique, Technical report, Bureau des Recherches Géologiques et Minières.

Bernard, M.-L., Coutant, O. & Beauducel, F., 2014. New insights on the structure of La Soufrière dome from joint inversion of P-wave velocity and density, in *EGU General Assembly Conference Abstracts,* Vol. 16, Copernicus Publications, p. 13205.

Bézèlgues-Courtade, S. & Bes-De-Berc, S., 2007. Inventaire et caractérisation des sources thermales de Guadeloupe, Tech. rep., Bureau des Recherches Géologiques et Minières.

Blakely, R.J., 1995. *Potential Theory in Gravity and Magnetic Applications,* Cambridge Univ. Press.

Boichu, M., Villemant, B. & Boudon, G., 2011. Degassing at La Soufrière de Guadeloupe volcano (Lesser Antilles) since the last eruptive crisis in 1975-77: result of a shallow magma intrusion?, *J. Volcanol. Geotherm. Res.,* **203,** 102–112.

Boudon, G., Komorowski, J.-C., Villemant, B. & Semet, M.P., 2008. A new scenario for the last magmatic eruption of La Soufrière of Guadeloupe (Lesser Antilles) in 1530 A.D. Evidence from stratigraphy radiocarbon dating and magmatic evolution of erupted products, *J. Volcanol. Geotherm. Res.,* **178,** 474–490.

Boulanger, O. & Chouteau, M., 2001. Constraints in 3D gravity inversion, *Geophys. Prospect.,* **49,** 265–280.

Bouysse, P., Mascle, A., Mauffret, A., Mercier de Lepinay, B., Jany, I., Leclere-Vanhoeve, A. & Montjaret, M.-C., 1988. Reconnaissance de structures tectoniques et volcaniques sous-marines de l'arc récent des Petites Antilles (Kick'em Jenny, Qualibou, Montagne Pelée, Nord-Ouest de la Guadeloupe), *Mar. Geol.,* **81,** 261–287.

Brombach, T., Marini, L. & Hunziker, J.C., 2000. Geochemistry of the thermal springs and fumaroles of Basse-Terre island, Guadeloupe, Lesser Antilles, *Bull. Volcanol.,* **61,** 477–490.

Camacho, A.G., Montesinos, F.G. & Vieira, R., 1997. A three-dimensional gravity inversion applied to São Miguel island (Azores), *J. geophys. Res.,* **102**(B4), 7717–7730.

Camacho, A.G., Montesinos, F.G. & Vieira, R., 2000. Gravity inversion by means of growing bodies, *Geophysics,* **65**(1), 95–101.

Camacho, A.G., Nunes, J.C., Ortiz, E., Frana, Z. & Vieira, R., 2007. Gravimetric determination of an intrusive complex under the Island of Faial (Azores): some methodological improvements, *Geophys. J. Int.,* **171,** 478–494.

Camacho, A.G., Fernández, J., González, P.J., Rundle, J.B., Prieto, J.F. & Arjona, A., 2009. Structural results for La Palma island using 3-D gravity inversion, *J. geophys. Res.,* **114,** B05411, doi:10.1029/2008JB005628.

Camacho, A.G., Fernández, J. & Gottsmann, J., 2011. A new gravity inversion method for multiple subhorizontal discontinuity interfaces and shallow basins, *J. geophys. Res.,* **116,** B02413, doi:10.1029/2010JB008023.

Carlut, J., Quidelleur, X., Courtillot, V. & Boudon, G., 2000. Paleomagnetic directions and K/Ar dating of 0 to 1 Ma lava flows from La Guadeloupe Island (French West Indies): implications for time-averaged field models, *J. geophys. Res.,* **105**(B1), 835–849.

Cella, F., Fedi, M., Florio, G., Grimaldi, M. & Rapolla, A., 2007. Shallow structure of the Somma–Vesuvius volcano from 3D inversion of gravity data, *J. Volcanol. Geotherm. Res.,* **161,** 303–317.

Collet, O., 2010. Utilisation de la corrélation de bruit sismique pour l'inversion d'un modèle de vitesse du dôme de la Soufrière, Guadeloupe, *Master's thesis,* École et Observatoire des Sciences de la Terre, Université de Strasbourg et Laboratoire de Géophysique Interne et Tectonophysique, Université Joseph-Fourier, Grenoble.

Coron, S., Feuillard, M. & Lubart, J.M., 1975. Études gravimétriques en Guadeloupe et dans les îles de son archipel - Petites Antilles, *Ann. Geophys.,* **31,** 531–548.

Coutant, O., Bernard, M.L., Beauducel, F., Nicollin, F., Bouin, M.P. & Roussel, S., 2012. Joint inversion of P-wave velocity and density, application to La Soufrière of Guadeloupe hydrothermal system, *Geophys. J. Int.,* **191,** 723–742.

Debeglia, N., Dupont, F. & Jousset, P., 2007. Surveillance gravimtrique du rservoir gothermique de Bouillante (Guadeloupe) - Annes 2006–2007, Technical report, Bureau des Recherches Géologiques et Minières.

Dentith, M. & Mudge, S.T., 2014. *Geophysics for the Mineral Exploration Geoscientist,* Cambridge Univ. Press.

Deplus, C., Le Friant, A., Boudon, G., Komorowski, J.-C., Villemant, B., Harford, C., Ségoufin, J. & Cheminée, J.-L., 2001. Submarine evidence for large-scale debris avalanches in the Lesser Antilles arc, *Earth planet. Sci. Lett.,* **192**(2), 145–157.

Dorel, J., Eschenbrenner, S. & Feuillard, M., 1979. Coupes sismiques des structures superficielles dans les Petites Antilles - I: Guadeloupe, *Pure appl. Geophys.,* **117,** 1050–1063.

Feuillard, M., 1976. Études thermiques à la Soufrière de la Guadeloupe, *Bull. BRGM,* **IV**(4), 375–388.

Feuillet, N., Manighetti, I., Tapponnier, P. & Jacques, E., 2002. Arc parallel extension and localization of volcanic complexes in Guadeloupe, Lesser Antilles, *J. geophys. Res.,* **107**(B12), ETG 3-1–ETG 3-29.

Feuillet, N. *et al.*, 2010. Active faulting induced by slip partitioning in Montserrat and link with volcanic activity: new insights from the 2009 GWADASEIS marine cruise data, *Geophys. Res. Lett.,* **37,** L00E15, doi:10.1029/2010GL042556.

Gailler, L.-S., Martelet, G., Thinon, I., Bouchot, V., Lebrun, J.-F. & Munch, P., 2013. Crustal structure of Guadeloupe island and the Lesser Antilles arc from a new gravity and magnetic synthesis, *Bull. Soc. Géol. Fr.,* **184**(1–2), 77–97.

Gailler, L.-S., Bouchot, V., Martelet, G., Thinon, I., Coppo, N., Baltassat, J.-M. & Bourgeois, B., 2014. Contribution of multi-method geophysics to the understanding of a high-temperature geothermal province: the Bouillante area (Guadeloupe, Lesser Antilles), *J. Volcanol. Geotherm. Res.,* **275,** 34–50.

García-Abdeslem, J. & Martín-Atienza, B., 2001. A method to compute terrain corrections for gravimeter stations using a digital elevation model, *Geophysics,* **66**(4), 1110–1115.

Green, W.R., 1975. Inversion of gravity profiles by use of a Backus-Gilbert approach, *Geophysics,* **40**(5), 763–772.

Guillen, A. & Menichetti, V., 1984. Gravity and magnetic inversion with minimization of a specific functional, *Geophysics,* **49**(8), 1354–1360.

Gunawan, H., 2005. Gravimétrie et microgravimétrie appliquées à la volcanologie: Exemples de la Soufrière de Guadeloupe et du Mépari, *PhD thesis,* Institut de Physique du Globe de Paris, Paris, France.

Hackney, R.I. & Featherstone, W.E., 2003. Geodetic versus geophysical perspectives of the 'gravity anomaly', *Geophys. J. Int.,* **154,** 35–43.

Hofmann-Wellenhof, B. & Moritz, H., 2005. *Physical Geodesy,* Springer.

Komorowski, J.-C., Boudon, G., Semet, M., Beauducel, F., Anténor-Habazac, C., Bazin, S. & Hammouya, G., 2005. Guadeloupe, in *Volcanic Hazard Atlas of The Lesser Antilles,* pp. 65–102, ed. Lindsay, J.M., Robertson, R.E.A., Shepherd, J.B. & Ali, S., Seismic Research Centre.

Lahitte, P., Samper, A. & Quidelleur, X., 2012. DEM-based reconstruction of southern Basse-Terre volcanoes (Guadeloupe archipelago, FWI): contribution to the Lesser Antilles Arc construction rates and magma production, *Geomorphology,* **136,** 148–164.

Last, B.J. & Kubik, K., 1983. Compact gravity inversion, *Geophysics,* **48**(6), 713–721.

Le Borgne, E. & Le Mouël, J.L., 1976. *Le levé aéromagnétique des Antilles franaises,* observations magnétiques, Vol. 26, Publications IPGP.

Le Mouël, J.L., Pozzi, J.P., Rossignol, J.-C. & Feuillard, M., 1979. Le levé aéromagnétique de l'archipel de Guadeloupe: description et implications tectoniques, *Bull. Soc. Géol. Fr.,* **21**(2), 135–148.

Lesparre, N., Gibert, D. & Marteau, J., 2012. Density muon radiography of La Soufrière of Guadeloupe volcano: comparison with geological, electrical resistivity and gravity data, *Geophys. J. Int.,* **185,** 1–14.

Lesparre, N., Grychtol, B., Gibert, D., Komorowski, J.-C. & Adler, A., 2014. Cross-section electrical resistance tomography of La Soufrière of Guadeloupe lava dome, *Geophys. J. Int.,* **197**(3), 1516–1526.

Lévêque, J.-J., Rivera, L. & Wittlinger, G., 1993. On the use of the checkerboard test to assess the resolution of tomographic inversions, *Geophys. J. Int.,* **115,** 313–318.

Li, X. & Götze, H.-J., 2001. Tutorial - Ellipsoid, geoid, gravity, geodesy, and geophysics, *Geophysics,* **66**(6), 1660–1668.

Li, Y. & Oldenburg, D.W., 1998. 3-D inversion of gravity data, *Geophysics,* **63**(1), 109–119.

Linde, N., Baron, L., Finizola, A., Revil, A., Muccini, F., Cocchi, L. & Carmisciano, C., 2014. 3-D density structure and geological evolution of Stromboli volcano (Aeolian Islands, Italy) inferred from land-based and sea-surface gravity data, *J. Volcanol. Geotherm. Res.,* **273,** 58–69.

Liuni, M.P., Loddo, M. & Schiavone, D., 2010. Non-linear inversion using a hybrid global search algorithm: applications in gravimetry, in *EGM 2010 International Workshop,* Capri, Italy.

Longman, I.M., 1959. Formula for computing the tidal accelerations due to the Moon and the Sun, *J. geophys. Res.,* **64**(12), 2351–2355.

MacCarthy, J.K., Borchers, B. & Aster, R.C., 2011. Efficient stochastic estimation of the model resolution matrix diagonal and general cross-validation for large geophysical inverse problems, *J. geophys. Res.,* **116,** B10304, doi:10.1029/2011JB008234.

Maceira, M. & Ammon, C.J., 2009. Joint inversion of surface wave velocity and gravity observations and its application to central Asian basins shear velocity structure, *J. geophys. Res.,* **114,** B02314, doi:10.1029/2007JB005157.

Marcotte, D., Shamsipour, P., Coutant, O. & Chouteau, M., 2014. Inversion of potential fields on nodes for large grids, *J. appl. Geophys.,* **110,** 90–97.

Mathieu, L., van Wyk de Vries, B., Pilato, M. & Troll, V.R., 2011. The interaction between volcanoes and strike-slip, transtensional and transpressional fault zones: analogue models and natural examples, *J. Struct. Geol.,* **33,** 898–906.

Mathieu, L., van Wyk de Vries, B., Mannessiez, C., Mazzoni, N., Savry, C. & Troll, V.R., 2013. The structure and morphology of the Basse Terre Island, Lesser Antilles volcanic arc, *Bull. Volcanol.,* **75,** 700, doi:10.1007/s00445-013-0700-y.

Matthieu, F., Pajot, G., Debeglia, N., Jousset, P., Dupont, F.D.L. & Franois, B., 2011. Surveillance gravimétrique du réservoir géothermique de Bouillante (Guadeloupe) - Année 2006–2010., Technical report, Bureau des Recherches Géologiques et Minières.

Menke, W., 1989. *Geophysical Data Analysis: Discrete Inverse Theory,* Academic Press.

Monteiller, V., 2005. Tomographie à l'aide de décalages temporels d'ondes sismiques P: développements méthodologiques et applications, *PhD thesis,* Université de Savoie.

Montesinos, F.G., Arnoso, J., Benavent, M. & Vieira, R., 2006. The crustal structure of El Hierro (Canary Island) from 3-D gravity inversion, *J. Volcanol. Geotherm. Res.,* **150,** 283–299.

Nicollin, F., Gibert, D., Beauducel, F., Boudon, G. & Komorowski, J.-C., 2006. Electrical tomography of La Soufrière of Guadeloupe volcano: field experiments, 1D inversion and qualitative interpretation, *Earth planet. Sci. Lett.,* **244,** 709–724.

Oliver, D.S., 1998. Calculation of the inverse of the covariance, *Math. Geol.,* **30**(7), 911–933.

Onizawa, S., Mikada, H., Watanabe, H. & Sakashita, S., 2002. A method for simultaneous velocity and density inversion and its application to and exploration of subsurface structure beneath Izu-Oshima volcano and Japan, *Earth Planets Space,* **54,** 803–817.

Parasnis, D.S., 1972. *Principles of Applied Geophysics,* Chapman and Hall.

Pavlis, N.K., Holmes, S.A., Kenyon, S.C. & Factor, J.K., 2008. An Earth Gravitational Model to degree 2160: EGM2008, in *General Assembly of the European Geosciences Union,* Vienna, Austria.

Pedersen, L.B., 1979. Constrained inversion of potential field data, *Geophys. Prospect.,* **27,** 726–748.

Pozzi, J.P., Le Mouël, J.L., Rossignol, J.C. & Zlotnicki, J., 1979. Magnetic observations made on La Soufrière volcano (Guadeloupe) during the 1976–1977 crisis, *J. Volcanol. Geotherm. Res.,* **5,** 217–137.

Represas, P., Catalão, J., Montesinos, F.G., Madeira, J., Mata, J., Antunes, C. & Moreira, M., 2012. Constraints on the structure of Maio Island (Cape Verde) by a three-dimensional gravity model: imaging partially exhumed magma chambers, *Geophys. J. Int.,* **190,** 931–940.

Sailhac, P. & Gibert, D., 2003. Identification of sources of potential fields with the continuous wavelet transform: two-dimensional wavelets and multipolar approximations, *J. geophys. Res.,* **108**(B5), 2262, doi:10.1029/2002JB002021.

Samper, A., Quidelleur, X., Lahitte, P. & Mollex, D., 2007. Timing of effusive volcanism and collapse events within an oceanic arc island: Basse-Terre, Guadeloupe archipelago (Lesser Antilles Arc), *Earth planet. Sci. Lett.,* **258,** 175–191.

Shamsipour, P., Marcotte, D., Chouteau, M. & Keating, P., 2010. 3D stochastic inversion of gravity data using cokriging and cosimulation, *Geophysics,* **75**(1), I1–I10.

Tarantola, A., 2005. *Inverse Problem Theory and Methods for Model Parameter Estimation,* SIAM.

Tarantola, A. & Valette, B., 1982. Inverse problems = Quest for information, *J. Geophys.,* **50,** 159–170.

The International Gravimetric Bureau (BGI), 2012. IAG Geodesist's Handbook, *J. Geod.,* **86**(10), 787–974.

Tiberi, C., Diament, M., Déverchère, J., Petit-Mariani, C., Mikhailov, V., Tikhotsky, S. & Achauer, U., 2003. Deep structure of the Baikal rift zone revealed by joint inversion of gravity and seismology, *J. geophys. Res.,* **108**(B3), 2133, doi:10.1029/2002JB001880.

Trampert, J., Fichtner, A. & Ritsema, J., 2013. Resolution tests revisited: the power of random numbers, *Geophys. J. Int.,* **192,** 676–680.

Tsuboi, C., 1983. *Gravity,* George Allen & Unwin (Publishers) Ltd.

Wang, C., Dong, S. & Munoz, E., 2010. Seawater density variations in the North Atlantic and the Atlantic meridional overturning circulation, *Clim. Dyn.,* **34,** 953–968.

Zlotnicki, J. & Nishida, Y., 2003. Review on morphological insights of self-potential anomalies on volcanoes, *Surv. Geophys.,* **24,** 291–338.

Zlotnicki, J., Vargemezis, G., Mille, A., Bruère, F. & Hammouya, G., 2006. State of the hydrothermal activity of Soufrière of Guadeloupe volcano inferred by VLF surveys, *J. appl. Geophys.,* **58,** 265–279.